

Two Reduced Models of Nerve Behavior

Joshua Rasband

A senior thesis submitted to the faculty of
Brigham Young University
in partial fulfillment of the requirements for the degree of
Bachelor of Science

Mark Transtrum, Advisor

Department of Physics and Astronomy
Brigham Young University

Copyright © 2021 Joshua Rasband

All Rights Reserved

ABSTRACT

Two Reduced Models of Nerve Behavior

Joshua Rasband

Department of Physics and Astronomy, BYU

Bachelor of Science

Predictive models are key to understanding the behavior of physical systems. Effective models can facilitate understanding of a complicated system. Ineffective models may have a large number of parameters, leading to the phenomenon of sloppiness, characterized by large uncertainties in estimating parameter values from data. Sloppiness has previously been observed in many fields, including power systems, chemical kinetics, and systems biology. We observe that the Hodgkin-Huxley model, a canonical model of the action potential in the giant squid axon, is a sloppy model. We describe the Manifold Boundary Approximation Method (MBAM), a technique for general model reduction. We use MBAM to construct minimal versions of the Hodgkin-Huxley model of the action potential for two example behaviors. These minimal models can better inform large-scale simulation of neurons in addition to lending important insight into biologically conserved characteristics of the neuron.

Keywords: Hodgkin-Huxley, FitzHugh-Nagumo, model reduction, manifold boundary approximation method, sloppy model, parameter identifiability

ACKNOWLEDGMENTS

Many people have supported and helped me in diverse ways. This research wouldn't have been possible without the generous funding and support of the Brigham Young University Department of Physics and Astronomy. My advisor, Dr. Mark Transtrum, was a great coach and mentor in this research. Finally, my family and friends have been a constant source of inspiration, support, and validation. Thank you.

Contents

Table of Contents	vii
List of Figures	ix
1 Introduction	1
1.1 Philosophical Foundations	1
1.2 The Successes of Physics and Effective Models	2
1.3 Problems With Modeling the Brain	2
1.4 Neuroscience for Physicists	3
1.5 Models in Neuroscience	3
1.6 Sloppiness in the Hodgkin-Huxley Model	5
1.7 Problem Formulation	8
2 Methods	9
2.1 Definitions: The Model, Residuals, and Cost	9
2.2 The Model Manifold and Reduction by Boundaries	10
2.3 Parameter Space Transformation	11
2.4 Hodgkin-Huxley Model Definition	11
2.5 The Fisher Information Matrix	11
2.6 Geodesic Calculation	12
2.7 Nonlinear Fitting	13
2.8 Sample Demonstration	13
3 Results and Discussion	17
3.1 Description of Reduced Models	17
3.2 Sensitivity Analysis of Reduced Models	17
3.3 The Reduced Limit Cycle and FitzHugh-Nagumo Models	20
3.4 Local Sloppiness	20
3.5 Conclusion	21
Bibliography	23

Appendix A	Model Definitions	25
A.1	The Hodgkin-Huxley Model	25
A.2	The FitzHugh-Nagumo Model	27
A.3	The Reduced Transition Model	28
A.4	The Reduced Transition Model (Dimensionless)	28
A.5	The Reduced Limit Cycle Model	29
A.6	The Reduced Limit Cycle Model (Dimensionless)	29
Appendix B	Reduction Descriptions	31
B.1	The Transition Model	31
B.2	The Limit Cycle Model	33

List of Figures

1.1	A cartoon drawing of a neuron.	4
1.2	Hodgkin-Huxley transition and limit cycle behavior	6
1.3	Comparison of predictions of the Hodgkin-Huxley and FitzHugh-Nagumo models.	7
2.1	Partial demonstration of the Manifold Boundary Approximation Method (MBAM)	15
3.1	Full and reduced model predictions	18
3.2	Sensitivity analysis for dimensionless, seven-parameter reduced transition model	19

Chapter 1

Introduction

The human brain remains a poorly-understood system. Despite science's success in modeling large, complex systems, there are factors that make it difficult to model the brain. Here, I introduce the idea of effective models, illustrate some problems with modeling the brain, introduce the idea of sloppiness, and explain the question my research will answer.

1.1 Philosophical Foundations

Predictive models are key to scientific understanding. Without getting lost in the philosophical thicket of what constitutes “understanding,” scientific understanding can be thought of as identifying, measuring, and describing physical systems. Mathematics provides an excellent formalism for describing the behavior of systems. Physicists, armed with mathematics, have been remarkably (some would say unreasonably [1]) successful at describing and predicting many types of behavior at very different scales, from the interactions of subatomic particles to black hole mergers.

1.2 The Successes of Physics and Effective Models

One of the great successes of physics is its ability to accurately describe the macroscopic behavior of complex systems with just a few parameters. As an example, we consider the ideal gas. A microscopic description of a system of 10^{23} gas particles would require solving the Schrödinger equation for a system of 10^{23} atoms, an impossibility with finite computational resources. Making the assumptions that quantum effects are small and that the particle sizes are very small, we could treat the system classically as point masses and describe their motion with Newton's laws of motion. This is better, but the system is still too large to compute a numerical solution with finite computational resources. Finally, we make assumptions about the distributions of energy and momenta among the gas particles. At last, we are able to describe macroscopic behavior (volume, pressure) of the gas with convenient parameters (moles of gas particles, temperature, et cetera). The ideal gas law is an example of an **effective model** because it has a simple mathematical form and contains parameters with meaningful contributions to predictions. It's important to note, however, that the ideal gas law rests on a number of assumptions that don't always apply. For example, under high-pressure or low-temperature conditions, intermolecular forces may become significant and a more complete description is necessary. Despite the successes of the ideal gas law and other effective models, some systems remain poorly understood.

1.3 Problems With Modeling the Brain

There is no effective model of the entire human brain, despite decades of concerted effort. Part of the problem is **complexity**. The brain has tens of billions of neurons with tens to hundreds of trillions of synaptic connections [2]. Even with incredible advances in computational resources, modeling the brain remains extremely computationally expensive. Another problem is **variability**. Even though most healthy human brains have the same capacities for vision, speech, and abstract

thought, individuals differ greatly in the precise wiring of their nervous system. Moreover, within an individual there is variation as neurons are born, grow, adapt, and die over the individual's lifetime. Especially during childhood and adolescence, neurons rapidly and dynamically change the ways that they are connected to each other. Finally, the same types of statistical assumptions that worked for the ideal gas don't work for the brain. The brain has no equilibrium state, is heterogeneous, and spatially distant parts of the brain can have strong effects on each other. Despite these and other challenges, the search for an effective model continues. Similarities in human behavior despite microscopic variability in nervous structure indicate that there may be laws of brain function that do not depend heavily on the precise details of the structure of the brain.

1.4 Neuroscience for Physicists

Those with a background in neuroscience are welcome to skip this section, which is intended to serve as a primer for those unfamiliar with the nervous system. The nervous system is composed of neurons which are connected to each other via **synapses** and **dendrites**. Dendrites receive signals from the synapses of other neurons. Signals propagate along the nerve membrane as a wave of drastic change in electrochemical potential of the membrane. This change in electrochemical potential is accomplished as ions flow down their concentration gradients into or out of the cell (see Figure 1.1). Neuroscientists have used various mathematical models to try to understand the behavior of neurons.

1.5 Models in Neuroscience

Although there are no effective models of the entire brain, there are good models of neurons (e.g. [3]). The neuron is the fundamental unit of the brain. Each neuron has the capacity to send and receive electrical signals to and from other neurons. These electrical signals are created by the

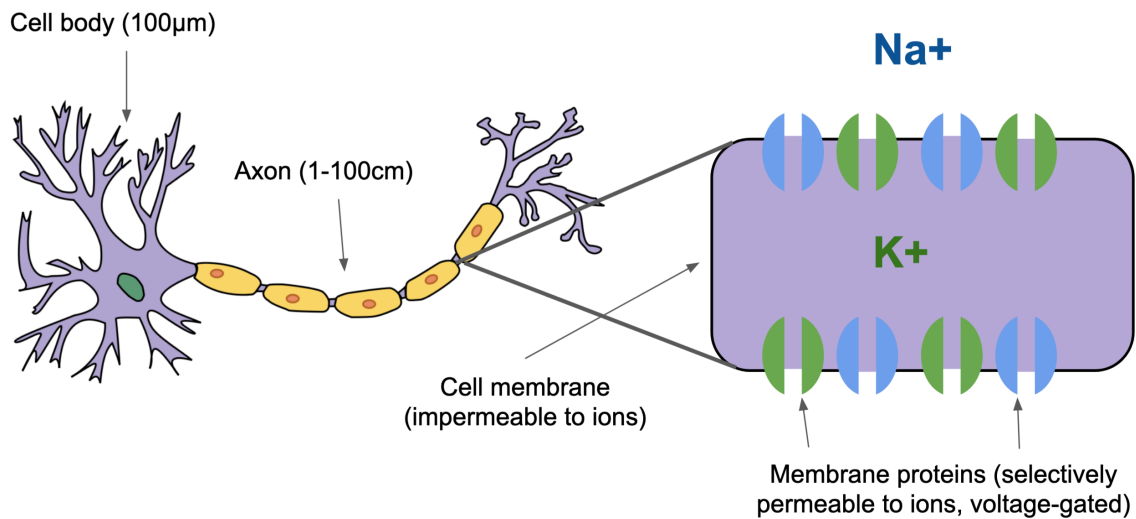


Figure 1.1 A cartoon drawing of a neuron. Modified, original from Wikimedia Commons, by Dhp1080, licensed under the [Creative Commons Attribution-Share Alike 3.0 Unported](#) license.

flow of ions across the cell membrane. The membrane has embedded proteins that act as channels or gates for the ions. Hodgkin and Huxley experimentally measured the kinetics of ion channels in response to externally applied potentials. The data were fit to Boltzmann equations, equations that describe the statistical behavior of a thermodynamic system in disequilibrium. Their results of their experiments were used to create the Hodgkin-Huxley model (Appendix A.1) [4], a physically motivated model of the membrane potential in nerve membrane. The Hodgkin-Huxley model has served as a template for many other modern conductance-based models.

Another model of nerve membrane potential is the FitzHugh-Nagumo model (Appendix A.2) [5]. Although both the Hodgkin-Huxley and FitzHugh-Nagumo models describe the same physical quantity — the resting membrane potential of the neuron — they are very different models. The Hodgkin-Huxley model may be considered a **mechanistic** model, a model which tries to capture microscopic physical processes and relationships. In contrast, the FitzHugh-Nagumo model may be considered a **phenomenological** model, a model which merely approximates macroscopic behavior

with a mathematical function. The differences between the equations of these two models (see Appendix A) illustrate the complimentary advantages and disadvantages of these two models. Although the Hodgkin-Huxley model is much more complicated than the FitzHugh-Nagumo model (25 parameters vs. 4 parameters, 4 differential equations vs. 2 differential equations), the Hodgkin-Huxley model has the advantage of describing the system in a physical, measurable way. The parameters of the Hodgkin-Huxley model correspond to real, measurable quantities. In contrast, the parameters of the FitzHugh-Nagumo model are dimensionless and it's less clear how they relate to characteristics of a physical system. The FitzHugh-Nagumo model is favored in many computational neuroscience applications because of its simplicity and decreased computational cost compared to the Hodgkin-Huxley model. Although not exhaustive, this brief comparison of the two models serves to illustrate their comparative advantages and disadvantages.

1.5.1 Example Behaviors and Comparison

The models can make a wide variety of predictions for different input currents and parameter values. Figure 1.2 shows the model predictions for two input currents. We call these behaviors the **transition** and **limit cycle** models, respectively. Figure 1.3 shows how the FitzHugh-Nagumo model approximates the Hodgkin-Huxley model very well for limit cycle behavior.

1.6 Sloppiness in the Hodgkin-Huxley Model

The Hodgkin-Huxley model is a model that exhibits sloppiness, a fact which was determined by the work of T. Bahr [6]. Sloppy models are models whose parameters are poorly constrained by data, leading to huge uncertainties in estimating parameter values. For parameters with huge uncertainties, there exist limiting approximations that eliminate the parameters from the model. The Manifold Boundary Approximation Method, a general algorithm for parameter reduction in sloppy models, is

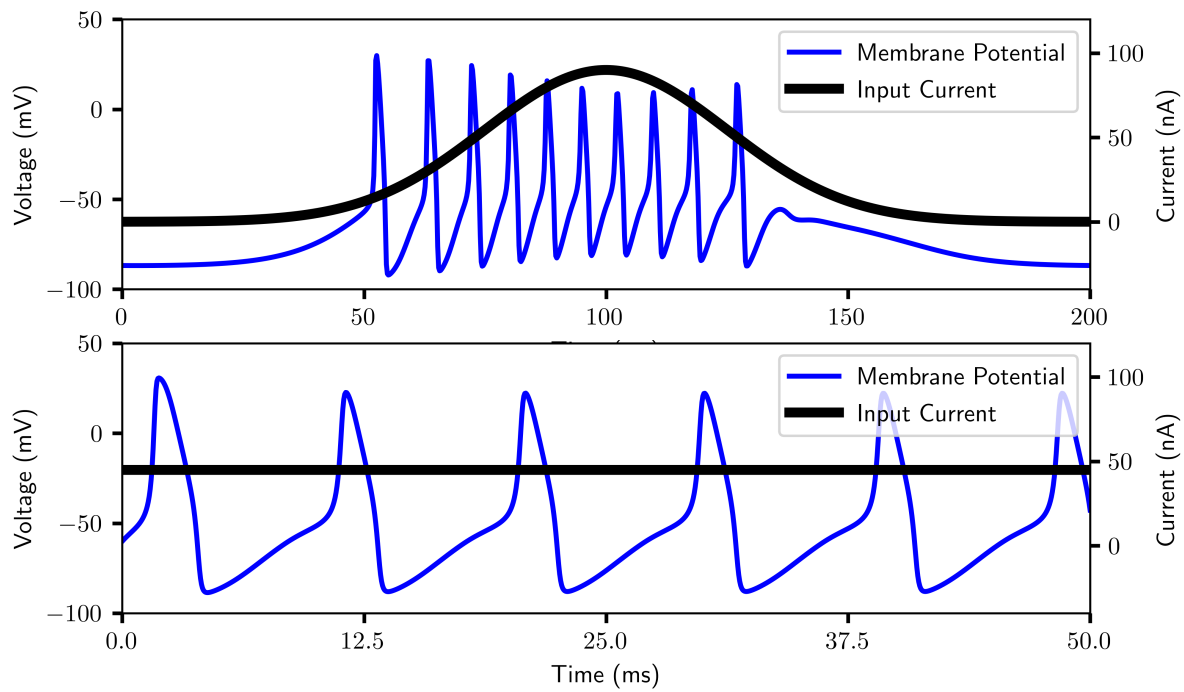


Figure 1.2 Demonstration of the transition and limit cycle behaviors in the Hodgkin-Huxley model

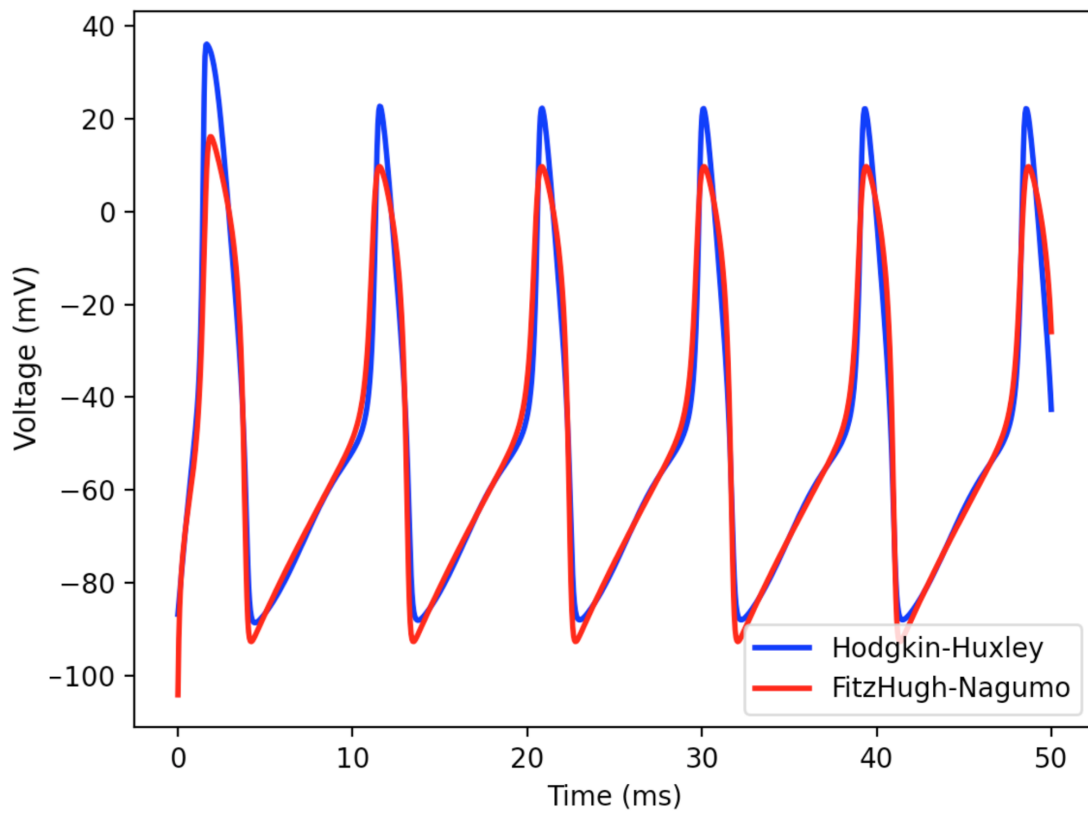


Figure 1.3 Comparison of predictions of the Hodgkin-Huxley and FitzHugh-Nagumo models.

described in Section 2. Bahr was able to use the Manifold Boundary Approximation Method to reduce the Hodgkin-Huxley model to fourteen parameters from its original twenty-six. My work extends his work by examining limit cycle behavior rather than only transition behavior.

1.7 Problem Formulation

I ask whether the FitzHugh-Nagumo model is a reduced form of the Hodgkin-Huxley model. That is, I attempt to discover some limiting assumptions for parameter values that result in a simplification of the Hodgkin-Huxley model to something more like the FitzHugh-Nagumo model. By discovering the parameter approximations for which the FitzHugh-Nagumo model's predictions approximate the Hodgkin-Huxley model well, one can determine under what conditions the FitzHugh-Nagumo model is appropriate to use as a substitute for the full Hodgkin-Huxley formalism. This clearly identifies which model may be suited for a given modeling task. Additionally, identifying the parameter combinations in the Hodgkin-Huxley model that correspond to parameters in the FitzHugh-Nagumo model will give physical meaning to the parameters of the FitzHugh-Nagumo model.

Chapter 2

Methods

The Manifold Boundary Approximation Method (MBAM) is an iterative technique for model reduction. It has been previously described in detail [7, 8]. Here, we discuss the theoretical basis of MBAM, describe its implementation for the Hodgkin-Huxley model, and give a sample demonstration.

2.1 Definitions: The Model, Residuals, and Cost

We begin with definitions. For a given system, we may experimentally measure data points $\{y_m\}$ sampled over an independent variable t at points $\{t_m\}$. A model is a function f with parameters $\theta = \{\theta_n\}$ that control model behavior. The model may be considered effective for describing the system if the predicted values $f(t_m, \theta)$ are close to the experimentally observed data $\{y_m\}$. As a preliminary step to optimizing parameter values for given data, we introduce the residuals:

$$r_m(\theta) = y_m - f(t_m, \theta). \quad (2.1)$$

Individual weights $\{\sigma_m\}$ can be assigned to data points, in which case the residuals become:

$$r_m(\theta) = \frac{y_m - f(t_m, \theta)}{\sigma_m}. \quad (2.2)$$

The sum of squares of residuals quantifies difference between model predictions and experimental observations. This metric, called the cost C is defined:

$$C(\theta) = \frac{1}{2} \sum_m [r_m(\theta)]^2. \quad (2.3)$$

With the cost as a function of parameter values for given experimental data, optimizing parameter values to fit a model to data becomes a cost minimization problem. We use a modified version of the Levenberg-Marquardt algorithm [9, 10] for fitting our models to data.

2.2 The Model Manifold and Reduction by Boundaries

Another interesting feature of the model is the set of all predictions available to the model for different parameter values. This set of all predictions is a high-dimensional object in the prediction space called the model manifold. It is visualized by using the model to map the entire parameter space into the prediction space.

Some models have a large number of parameters, some or most of which are poorly constrained when fit to experimental data. Such models with huge uncertainties in parameter values are called sloppy models. Sloppy models have been identified in many fields, including power systems, chemical kinetics, and systems biology [11]. The model manifold for a sloppy model is bounded by a hierarchy of widths spanning many orders of magnitude. The boundaries of the model may be used as submanifold approximations to the full model manifold. These geometric approximations to the model manifold have a symbolic interpretation as reduced forms of the original model, created by pushing parameter values to extremes.

Starting at an initial point on the model manifold, representing a prediction for an initial set of parameter values, we may calculate a path to the nearest boundary of the manifold. This path is called a geodesic. After reaching the closest boundary, we fit the model on the boundary by minimizing the cost. If the distance traveled from the initial point to the point on the boundary is sufficiently

small, as measured by the cost function, we say that the boundary is a good approximation of the original manifold. This process can be repeated for the boundary, which is itself a reduced model manifold. Once the distance to a boundary is too large there are no longer any reduced models that make good predictions.

2.3 Parameter Space Transformation

Because parameter values can get very large on the boundaries of the model manifold, it is convenient to transform the parameters. If the parameter can have only positive, nonzero values, a logarithmic transformation “shrinks” that axis of parameter space for convenience during numerical calculation, as well as ensuring that the parameter can never take forbidden values during calculation. Similarly, a hyperbolic sine transformation may be used for parameters that can take both positive and negative values.

2.4 Hodgkin-Huxley Model Definition

The Hodgkin-Huxley model was implemented in the Julia programming language, using the Sundials package for finding numerical solutions to differential equations. These packages were developed by the Transtrum research group for their accessibility and high performance.

2.5 The Fisher Information Matrix

The Fisher Information Matrix g is a metric for the model manifold. It is defined by $g = J^T J$, where J is the Jacobian matrix. Elements of the Jacobian are calculated as the derivative of residuals with respect to parameter values:

$$J_{m\mu} = \frac{\partial r_m}{\partial \theta_\mu} = \partial_\mu r_m \quad (2.4)$$

The largest eigenvalues of the Fisher Information Matrix correspond to parameters which are most important for determining model behavior. (The eigenvalues of the Fisher Information Matrices for the full and reduced Hodgkin-Huxley models are graphed in Figure 3.1c, d.)

2.6 Geodesic Calculation

The calculation of the geodesic is described in detail in [7] (especially Section VI). Here, we reproduce the essentials of geodesic calculation. The geodesic is the shortest path between two points on a manifold. The parameters corresponding to a geodesic path can be found by solving the differential equation

$$\ddot{x}^\mu + \Gamma_{\alpha\beta}^\mu \dot{x}^\alpha \dot{x}^\beta = 0 \quad (2.5)$$

where $\Gamma_{\alpha\beta}^\mu$ are the connection coefficients calculated from the metric of the manifold and the dot means differentiation with respect to the curve's affine parameterization. The connection coefficients are defined according to

$$\Gamma_{\mu\nu}^\alpha = \frac{1}{2} g^{\alpha\beta} (\partial_\mu g_{\beta\nu} + \partial_\nu g_{\beta\mu} - \partial_\beta g_{\mu\nu}) \quad (2.6)$$

where g is the metric. The connection coefficients may also be defined in terms of the residuals

$$\Gamma_{\mu\nu}^\alpha = g^{\alpha\beta} \sum_m \partial_\beta r_m \partial_\mu \partial_\nu r_m. \quad (2.7)$$

In our implementation, we used automatic differentiation to calculate a geodesic path. The direction of the geodesic was chosen to correspond to the direction that had the least effect on model predictions, i.e., corresponding to the smallest eigenvalue of the Fisher Information Matrix.

2.6.1 Einstein Summation Convention

This section briefly explains the use of Einstein notation for those who may be unfamiliar with it. In the Einstein summation convention, the occurrence of the same subscript and superscript index

variable in a term indicates an implied sum over the index. In the geodesic calculation, the indices are coordinates in a coordinate system. This convention results in much more concise algebraic formulae. A detailed explanation of the convention is beyond the scope of this thesis.

2.7 Nonlinear Fitting

Models were fit using a Levenberg-Marquardt algorithm [9]. In brief, the modified Levenberg-Marquardt algorithm is an adaptive algorithm for nonlinear least-squares fitting. It interpolates between the Gauss-Newton algorithm and gradient descent, two early approaches to least-squares fitting.

2.8 Sample Demonstration

We demonstrate elements of MBAM using the Hodgkin-Huxley model. First we pick three timepoints at which to sample our model (Figure 2.1b). These timepoints correspond to the axes of the prediction space (Figure 2.1a). Next, we pick two parameters from which to form our parameter space (Figure 2.1c). Note that the selection of only three timepoints and two parameters is done so this example reduction may be easily visualized. In full MBAM, there are 1001 sampled timepoints and many more parameters.

The model manifold is created by using the model to map the parameter space to the prediction space (Figure 2.1a). Every point in the parameter space corresponds to a point in prediction space. The resulting model manifold in this case is a thin, two-dimensional sheet or ribbon. It is much wider in some directions than in others. The wide directions correspond to parameters or parameter combinations which are important for determining model behavior, while the narrow directions correspond to less important parameters. In this sample demonstration, we have identified the red edge as the edge closest to the initial point on the manifold. The red edge corresponds to the limit

of the model as K_{β_n} approaches infinity. Note in Figure 2.1c, which shows the cost surface as parameter values are varied, the “canyon” of low cost as the parameter K_{β_n} is pushed to very large values. This limit corresponds to the same edge of the model manifold highlighted in red. The low cost of pushing K_{β_n} to extreme values indicates that the reduced model obtained by the limit of the model as K_{β_n} approaches infinity gives predictions that are close to the original predictions.

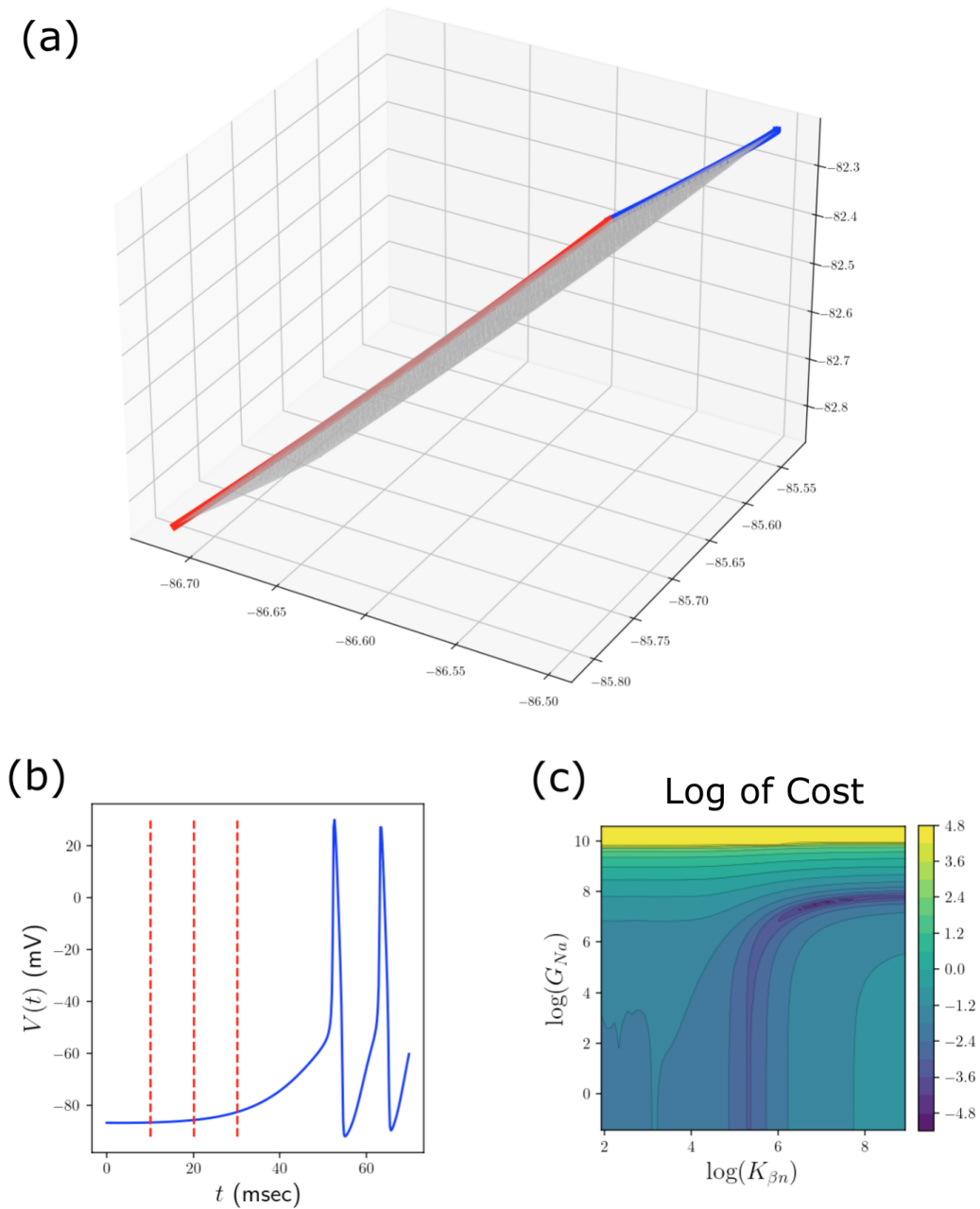


Figure 2.1 Partial demonstration of the Manifold Boundary Approximation Method (MBAM). (a) The model manifold, a surface created by plotting model predictions for each of the three time points as model parameter values are varied. (b) Three time points are selected for calculating and plotting the cost surface (c) and model manifold (a). (c) Cost contour plot as model parameter values are varied.

Chapter 3

Results and Discussion

3.1 Description of Reduced Models

By applying MBAM to the full Hodgkin-Huxley model, we were able to obtain greatly reduced models for the two types of data studied. The model of a transition from resting to spiking was reduced to ten parameters, while the model of limit cycle spiking was reduced to seven parameters. The full model definitions are given in Appendix A.

Figure 3.1 demonstrates full and reduced model predictions. Even with the majority of parameters eliminated from the models, they are still able to reproduce important features of full model behavior.

3.2 Sensitivity Analysis of Reduced Models

Each parameter in the reduced models is associated with some unique capacity of the model to vary predictions. By slightly changing parameter values one parameter at a time, we can learn how changes in parameter values affect model behavior.

Figure 3.2 shows a qualitative sensitivity analysis for the reduced dimensionless transition

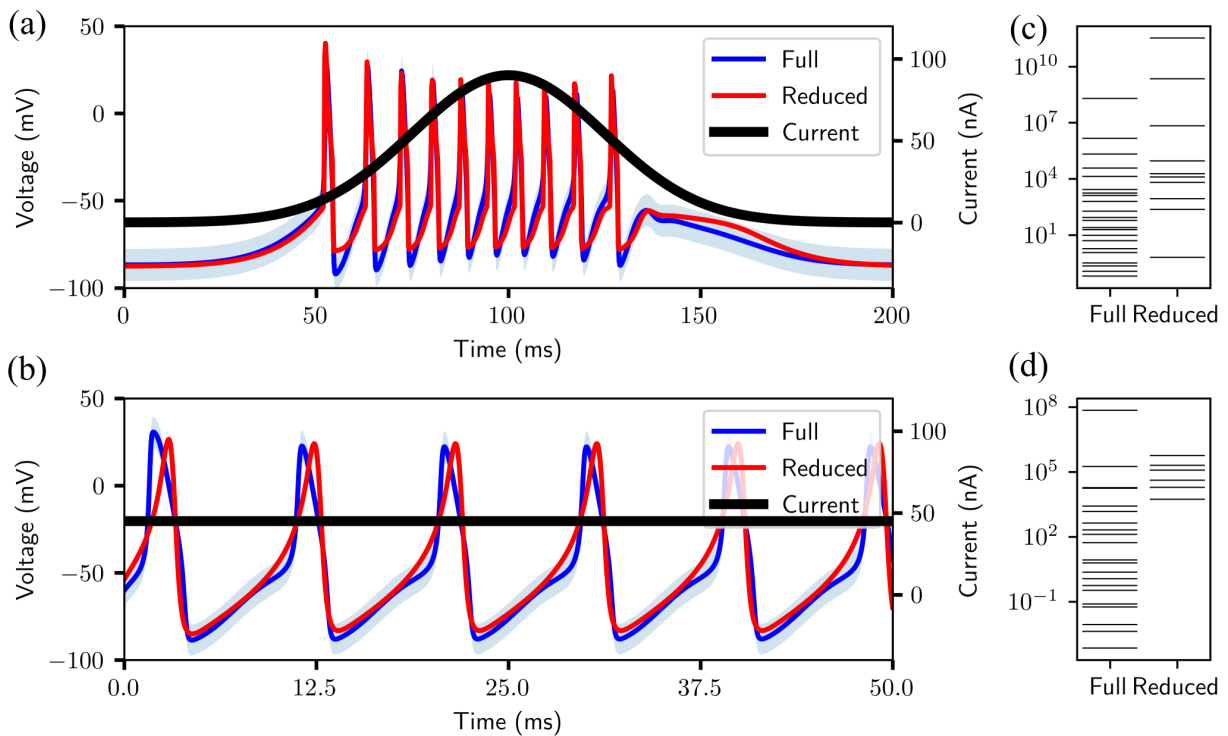


Figure 3.1 Overview of model predictions for a given applied current, with the eigenvalues of the Fisher Information Matrix for each model. Two types of applied current were studied. (a) A Gaussian "pulse" of input current shows a transition from a resting to a spiking state. (b) Constant input current shows limit-cycle behavior.

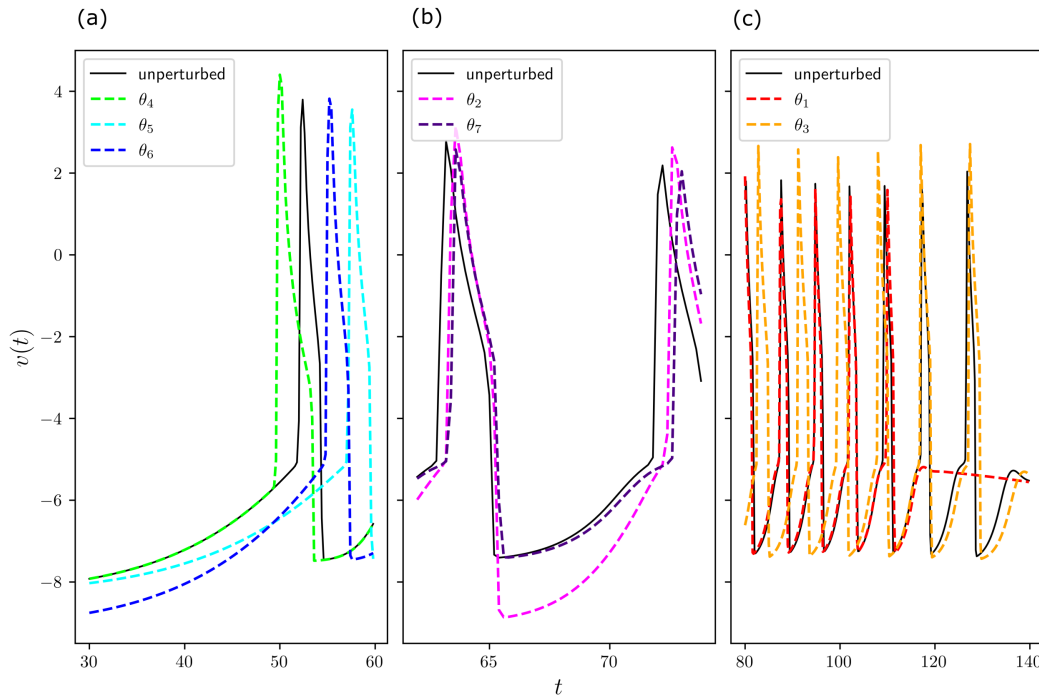


Figure 3.2 Sensitivity analysis for the dimensionless, seven-parameter reduced transition model (Appendix A.4).

model, described in Appendix A. The solid line indicates reduced model predictions for unperturbed parameter values. Each dashed line shows model predictions after one parameter has been slightly changed. Rather than showing an overview of all predictions, each panel focuses on time intervals that highlight the relevant changes in model predictions.

In Figure 3.2a, the parameters θ_4 , θ_5 , and θ_6 are adjusted. Inspection of their effects on model predictions shows that θ_4 controls the threshold voltage for spiking, θ_5 controls rate of change of voltage, and θ_6 controls equilibrium potential. Similarly, inspection of Figure 3.2b shows that θ_2 controls depth of hyperpolarization while θ_7 controls the length of the refractory period. Finally, Figure 3.2c shows that θ_1 and θ_3 are parameters that control for the duration of spiking and the frequency of spiking, respectively.

3.3 The Reduced Limit Cycle and FitzHugh-Nagumo Models

The reduced limit cycle and FitzHugh-Nagumo models have almost identical forms. This indicates that the FitzHugh-Nagumo model's parameters have physical correlates in the Hodgkin-Huxley model. A next step for our work will be to identify experimental conditions under which it is appropriate to use the FitzHugh-Nagumo model rather than a more complex model.

3.4 Local Sloppiness

Initial analysis of the eigenvalues of the Fisher Information Matrix (Figure 3.1c, d) indicated that we would be able to remove about half of the parameters in the model. As we iterated MBAM, the eigenvalues of the Fisher Information Matrix changed significantly. Sometimes eigenvalues increased, indicating parameters becoming more stiff, while other times eigenvalues decreased, indicating parameters becoming more sloppy. We believe that the shifts in eigenvalues are due to the phenomenon of *local sloppiness* which we observed while calculating geodesics. At some points on the model manifold, one parameter would appear to be very sloppy and the geodesic would move in that direction. After a while, the parameter became extremely stiff. Parameters representing potentials were particularly prone to being locally sloppy. The model was able to compensate for modifications to the threshold potential, up to a certain critical threshold, at which changes to the potential became extremely important for determining behavior. Locally sloppy parameters pose challenges for implementing MBAM automatically, without human oversight. More work is necessary to understand how local sloppiness occurs in models and how MBAM can be modified to detect and adapt to local sloppiness.

3.5 Conclusion

The reduced models described in Section 3.1 and Appendix A are a powerful demonstration of the capacity of MBAM to reduce unnecessary model complexity. Our success suggests that the Hodgkin-Huxley model (and similar mechanistic models) contain more information than is necessary for many common modeling applications.

This work represents a significant improvement in parameter reduction of the Hodgkin-Huxley model. Although previous work had established that the Hodgkin-Huxley model exhibits sloppiness, the limit cycle behavior of the Hodgkin-Huxley model had not yet been studied with MBAM [6]. Additionally, our work on the transition model eliminated four more parameters than previous work had been able to do.

Walch and Eisenberg noted the need for identifiability analysis in current-clamp experiments [12]. Our findings are a first investigation of parameter identifiability for the Hodgkin-Huxley model in current-clamp experiments. MBAM selects for the parameters and combinations of parameters that are able to be determined from data.

Although the two behaviors we studied capture important elements of typical neuron behavior, they are by no means exhaustive of the full range of behaviors available to the Hodgkin-Huxley model. Further work could very easily apply MBAM to interesting experimental conditions for the Hodgkin-Huxley model, such as altered initial parameter conditions or modified input currents. Additionally, the Hodgkin-Huxley model is only one model in a population of detailed, conductance-based models commonly used by computational neuroscientists. The methods outlined in Section 2 are general and will work for any conductance-based model. More work is necessary to understand how additional types of ionic channels will affect reduced model structure and behavior.

Bibliography

- [1] E. P. Wigner, “The Unreasonable Effectiveness of Mathematics in the Natural Sciences,” *Communications in Pure Applied Mathematics* **13**, 1–14 (1960).
- [2] C. S. von Bartheld, J. Bahney, and S. Herculano-Houzel, “The search for true numbers of neurons and glial cells in the human brain: a review of 150 years of cell counting,” *Journal of Comparative Neurology* **524**, 3865–3895 (2016).
- [3] F. Buchholtz, J. Golowasch, I. R. Epstein, and E. Marder, “Mathematical model of an identified stomatogastric ganglion neuron,” *Journal of neurophysiology* **67**, 332–340 (1992).
- [4] A. L. Hodgkin and A. F. Huxley, “A quantitative description of membrane current and its application to conduction and excitation in nerve,” *The Journal of physiology* **117**, 500 (1952).
- [5] R. FitzHugh, “Impulses and physiological states in theoretical models of nerve membrane,” *Biophysical journal* **1**, 445–466 (1961).
- [6] T. Bahr, undergraduate Senior Thesis (Brigham Young University Department of Physics and Astronomy) (unpublished).
- [7] M. K. Transtrum, B. B. Machta, and J. P. Sethna, “Geometry of nonlinear least squares with applications to sloppy models and optimization,” *Physical Review E* **83**, 036701 (2011).

- [8] M. K. Transtrum and P. Qiu, “Model reduction by manifold boundaries,” *Physical review letters* **113**, 098701 (2014).
- [9] D. W. Marquardt, “An algorithm for least-squares estimation of nonlinear parameters,” *Journal of the society for Industrial and Applied Mathematics* **11**, 431–441 (1963).
- [10] M. K. Transtrum and J. P. Sethna, “Improvements to the Levenberg-Marquardt algorithm for nonlinear least-squares minimization,” arXiv preprint arXiv:1201.5885 (2012).
- [11] M. K. Transtrum, B. B. Machta, K. S. Brown, B. C. Daniels, C. R. Myers, and J. P. Sethna, “Perspective: Sloppiness and emergent theories in physics, biology, and beyond,” *The Journal of chemical physics* **143**, 07B201_1 (2015).
- [12] O. J. Walch and M. C. Eisenberg, “Parameter identifiability and identifiable combinations in generalized Hodgkin–Huxley models,” *Neurocomputing* **199**, 137–143 (2016).
- [13] E. Buckingham, “On physically similar systems; illustrations of the use of dimensional equations,” *Physical review* **4**, 345 (1914).

Appendix A

Model Definitions

A.1 The Hodgkin-Huxley Model

The following description of the Hodgkin-Huxley model is adapted from [6]. The Hodgkin-Huxley model consists of four nonlinear coupled differential equations. They describe the dynamics of four variables: voltage V , potassium channel activation constant n , sodium channel activation constant m , and sodium channel inactivation constant h . The activation and inactivation constants, also called gating variables, describe the statistics of how many channels in a population of ion channels will be in the open configuration. Accordingly, the gating variables can take values between zero and unity. The time differential of voltage is given by

$$\frac{dV}{dt} = (I_{\text{app}} - I_K - I_{Na} - I_L)/C_m \quad (\text{A.1})$$

where

$$I_K = n^4 G_K (V - E_K) \quad (\text{A.2})$$

$$I_{Na} = m^3 h G_{Na} (V - E_{Na}) \quad (\text{A.3})$$

$$I_L = G_L (V - E_L) \quad (\text{A.4})$$

I_K , I_{Na} , and I_L represent the current passing through potassium, sodium, and leak channels, respectively. The G_x correspond to maximal conductances of the ion channels and are determined by channel structure and composition. (Conductance, a convenient unit in electrophysiology, is defined as the inverse of resistance.) The E_x correspond to electrochemical potentials that result from ion concentration gradients across the cell membrane. The membrane capacitance C_m is determined by cell geometry.

The differential equations for the gating variables are very similar, so we introduce an iterator i representing n , m , and h . Then the time differential of i is given by

$$\frac{di}{dt} = \frac{i - i_\infty}{\tau_i} \quad (\text{A.5})$$

where

$$i_\infty = \frac{A_i}{A_i + B_i} \quad (\text{A.6})$$

$$\tau_i = \frac{1}{A_i + B_i} \quad (\text{A.7})$$

where A_i , B_i are functions of V that vary for each n , m , h .

$$A_n = \frac{\alpha_n(V - V_{\alpha_n})}{1 - \exp[-(V - V_{\alpha_n})/K_{\alpha_n}]} \quad (\text{A.8})$$

$$A_m = \frac{\alpha_m(V - V_{\alpha_m})}{1 - \exp[-(V - V_{\alpha_m})/K_{\alpha_m}]} \quad (\text{A.9})$$

$$A_h = \alpha_h \exp[-(V - V_{\alpha_h})/K_{\alpha_h}] \quad (\text{A.10})$$

$$B_n = \beta_n \exp[-(V - V_{\beta_n})/K_{\beta_n}] \quad (\text{A.11})$$

$$B_m = \beta_m \exp[-(V - V_{\beta_m})/K_{\beta_m}] \quad (\text{A.12})$$

$$B_h = \frac{\beta_h}{1 + \exp[-(V - V_{\beta_h})/K_{\beta_h}]} \quad (\text{A.13})$$

Each α_x , β_x , V_x , and K_x is a parameter of the Hodgkin-Huxley model and characterize the dynamics of the ion channels. There are a total of 25 parameters in the Hodgkin-Huxley model.

$V_0 = -86.8$	$n_0 = 0.0537$	$m_0 = 0.00179$	$h_0 = 0.987$	$I_{\text{app}} = 90e^{-\left[\frac{(t-100)^2}{1250}\right]}$	$C_m = 1.0$
$G_K = 36.0$	$G_{Na} = 120.0$	$G_L = 0.30$	$E_K = -95.3$	$E_{Na} = 36.7$	$E_L = -87.0$
$V_{\alpha_n} = -50.0$	$V_{\alpha_m} = -36.0$	$V_{\alpha_h} = -60.0$	$V_{\beta_n} = -60.0$	$V_{\beta_m} = -60.0$	$V_{\beta_h} = -30.0$
$K_{\alpha_n} = 10.0$	$K_{\alpha_m} = 10.0$	$K_{\alpha_h} = 20.0$	$K_{\beta_n} = 80.0$	$K_{\beta_m} = 18.0$	$K_{\beta_h} = 10.0$
$\alpha_n = 0.01$	$\alpha_m = 0.1$	$\alpha_h = 0.07$	$\beta_n = 0.125$	$\beta_m = 4.0$	$\beta_h = 1.0$

Table A.1 Table of initial parameter values for the Hodgkin-Huxley model. See Appendix A.1.1 for units.

A.1.1 Initial Parameter Values for the Hodgkin-Huxley Model

The initial parameter values in the Hodgkin-Huxley model are given in Table A.1. Parameters of the form V_x , E_x , and K_x have units of milivolts, parameters of the form G_x have units of milisiemens (where a siemen is an inverse ohm, $1/\Omega$), C_m has units of microfarads, I_{app} has units of nanoamperes, parameters α_n and α_m have units of inverse milivolts miliseconds ($\text{mV}^{-1}\text{msec}^{-1}$), all other parameters of the form α_x or β_x have units of inverse miliseconds (msec^{-1}), and the gating variable initial conditions n_0 , m_0 , h_0 are dimensionless.

A.2 The FitzHugh-Nagumo Model

The FitzHugh-Nagumo model [5] is a phenomenological model of nerve excitation.

$$\dot{v} = v - v^3/3 - w + RI_{\text{ext}} \quad (\text{A.14})$$

$$\tau\dot{w} = v + a - bw \quad (\text{A.15})$$

The variable v is a dimensionless membrane potential, while w is a relaxation variable. The parameters a , b , τ , and RI_{ext} are dimensionless parameters, with τ being a time constant and RI_{ext} a term intended to correspond to externally applied current. There are a total of four dimensionless

parameters in the FitzHugh-Nagumo model.

A.3 The Reduced Transition Model

$$\dot{V} = [I_{\text{app}} - \tilde{G}_K \tilde{n}^4 (V - E_K) + I_{Na} \tilde{m}_\infty^3 \tilde{h}_\infty - G_L (V - E_L)] / C_m \quad (\text{A.16})$$

$$\dot{\tilde{n}} = \text{ReLU}(V - V_{\alpha_n}) - \tilde{\beta}_n \tilde{n} \quad (\text{A.17})$$

where

$$\tilde{m}_\infty = \text{ReLU}(V - V_{\alpha_m}) \quad (\text{A.18})$$

$$\tilde{h}_\infty = e^{-V/K_{\alpha_h}} \quad (\text{A.19})$$

$$\text{ReLU}(x) = x \mathcal{H}(x) \quad (\text{A.20})$$

and \mathcal{H} is the Heaviside step function. This reduced model has a total of ten parameters. There are three physical dimensions present in this model: voltage, time, and membrane capacitance. By the Buckingham π Theorem [13], this model can be transformed into a dimensionless model of seven dimensionless parameters.

A.4 The Reduced Transition Model (Dimensionless)

$$\dot{v} = \tilde{I}_{\text{app}} - \theta_1 w^4 (v - \theta_2) + \theta_3 e^{-v} [\text{ReLU}(v - \theta_4)]^3 - \theta_5 (v - \theta_6) \quad (\text{A.21})$$

$$\dot{w} = \text{ReLU}(v - \theta_7) - w \quad (\text{A.22})$$

where

$$\text{ReLU}(x) = x \mathcal{H}(x) \quad (\text{A.23})$$

and \mathcal{H} is the Heaviside step function.

A.5 The Reduced Limit Cycle Model

$$\dot{V} = -I_K \tilde{n}^4 + I_{Na} \{1 / (1 + \exp[-(V - V_{\beta_m}) / K_{\beta_m}])\}^3 \quad (\text{A.24})$$

$$\dot{\tilde{n}} = V - V_{\alpha_n} - \tilde{\beta}_n \tilde{n} \quad (\text{A.25})$$

A.6 The Reduced Limit Cycle Model (Dimensionless)

$$\dot{v} = -w^4 + \theta_1 \left(\frac{1}{1 + e^{-v}} \right)^3 \quad (\text{A.26})$$

$$\dot{w} = (v + \theta_2 - w) \theta_3 \quad (\text{A.27})$$

Appendix B

Reduction Descriptions

B.1 The Transition Model

We describe here, in order, the limits found via MBAM and used to reduce the number of parameters in the Hodgkin-Huxley model for a transition from resting to spiking to resting.

B.1.1 Treatment of Initial Conditions

Although initial conditions can be written as parameters in the model code, initial conditions are not “true” parameters in the sense that they do not define rules for how the system behaves, rather, they define the initial state of the system. In the transition model, we eliminated the initial conditions by using a steady-state approximation. The initial conditions were set to whatever values would result in the system being at equilibrium at time $t = 0$.

B.1.2 List of Reductions

1. 25 \rightarrow 22: Elimination of Structurally Unidentifiable Parameters

The parameters V_{α_n} , V_{β_n} , and V_{β_m} are structurally unidentifiable. They can be combined with

another parameter to create a single equivalent parameter with no loss of model fidelity. The parameters all appear in the form

$$X = xe^{-(V-V_x)/K_x}. \quad (\text{B.1})$$

We note that this is equivalent to

$$X = (xe^{V_x/K_x})e^{-V/K_x} = \tilde{x}e^{-V/K_x}. \quad (\text{B.2})$$

For each of the parameters V_{α_h} , V_{β_n} , and V_{β_m} , we can “absorb” them into their corresponding parameters α_h , β_n , and β_m to create the new parameters $\tilde{\alpha}_h$, $\tilde{\beta}_n$, and $\tilde{\beta}_m$. This elimination of structurally unidentifiable parameters occurs as a preliminary step to performing MBAM in both the transition and limit cycle models.

2. 22 \rightarrow 21: $K_{\beta_n} \rightarrow \infty$
3. 21 \rightarrow 20: $G_K \rightarrow \infty$, $\alpha_n^4 \rightarrow 0$, $G_K \alpha_n^4 \rightarrow \tilde{G}_K$
4. 20 \rightarrow 19: $G_{Na} \rightarrow \infty$, $\alpha_h \rightarrow 0$, $G_{Na} \alpha_h \rightarrow \tilde{G}_{Na}$
5. 19 \rightarrow 18: $\beta_h \rightarrow \infty$, $V_{\beta_h} \rightarrow \infty$, $\beta_h e^{-V_{\beta_h}/K_{\beta_h}} \rightarrow \tilde{\beta}_h$
6. 18 \rightarrow 17: $K_{\beta_h} \rightarrow \infty$
7. 17 \rightarrow 16: $K_{\beta_m} \rightarrow \infty$
8. 16 \rightarrow 15: $G_{Na} \rightarrow 0$, $\alpha_m^3 \rightarrow \infty$, $G_{Na} \alpha_m^3 \rightarrow \tilde{G}_{Na}$
9. 15 \rightarrow 14: $K_{\alpha_m} \rightarrow 0$
10. 14 \rightarrow 13: $G_{Na} \rightarrow 0$, $E_{Na} \rightarrow \infty$, $G_{Na} E_{Na} \rightarrow I_{Na}$
11. 13 \rightarrow 12: $\tau_h \rightarrow 0$, $h \rightarrow h_\infty$

12. $12 \rightarrow 11: K_{\alpha_n} \rightarrow 0$

13. $11 \rightarrow 10: \tau_m \rightarrow 0, m \rightarrow m_\infty$

14. $10 \rightarrow 7$: Removing Dimension

We describe briefly the process of obtaining the dimensionless transition model in Appendix A.4 from the reduced transition model in Appendix A.3. First, we pick a convenient definition for dimensionless voltage $v = V/K_{\alpha_h}$. Next, we find an appropriate dimensionless time, in this case $\tau = K_{\alpha_h}t$. Finally, we remove the dimension of capacitance, C_m . This process recovers seven dimensionless parameters:

$$\theta_1 = \frac{\tilde{G}_K K_{\alpha_h}^3}{\tilde{\beta}_n^4 C_m} \quad (\text{B.3})$$

$$\theta_2 = E_K / K_{\alpha_h} \quad (\text{B.4})$$

$$\theta_3 = \frac{I_{Na} K_{\alpha_h}}{C_m} \quad (\text{B.5})$$

$$\theta_4 = V_{\alpha_n} / K_{\alpha_h} \quad (\text{B.6})$$

$$\theta_5 = \frac{G_L}{K_{\alpha_h} C_m} \quad (\text{B.7})$$

$$\theta_6 = E_L / K_{\alpha_h} \quad (\text{B.8})$$

$$\theta_7 = V_{\alpha_m} / K_{\alpha_h} \quad (\text{B.9})$$

B.2 The Limit Cycle Model

We describe here, in order, the limits found via MBAM and used to reduce the number of parameters in the Hodgkin-Huxley model for limit cycle behavior.

B.2.1 Treatment of Initial Conditions

As in the transition model, initial conditions are not “true” parameters. The initial conditions don’t matter very much in the limit cycle case because we are concerned only about the limit cycle itself (amplitude, frequency, shape of cycle, et cetera). Any initial conditions that lead to limit cycle behavior are permissible, and any transient imperfections resulting from poorly-chosen initial conditions are not very concerning because we can use the limit cycle itself to find good values for initial conditions of the dynamical variables.

B.2.2 List of Reductions

1. 25 \rightarrow 21: Elimination of Structurally Unidentifiable Parameters As in the transition model, structurally unidentifiable parameters

V_{α_n} , V_{β_n} , and V_{β_m} can be eliminated. Additionally, the parameter C_m is structurally unidentifiable in this model because the applied current is constant in time. The applied current can be “absorbed” into the leak current I_L , by redefining I_L (and E_L) in the following way:

$$\tilde{I}_L = I_{\text{app}} - I_L = I_{\text{app}} - G_L(V - E_L) = -G_L[V - (E_L + I_{\text{app}}/G_L)] = -G_L(V - \tilde{E}_L) \quad (\text{B.10})$$

We can now redefine all G_x by $\tilde{G}_x = G_x/C_m$ and thus eliminate the parameter C_m from our model. It’s important to note that this changes the units of G_x , as they are no longer conductances but units of inverse time.

2. 21 \rightarrow 20: $K_{\beta_n} \rightarrow \infty$
3. 20 \rightarrow 19: $K_{\alpha_n} \rightarrow 0$
4. 19 \rightarrow 18: $G_K \rightarrow \infty$, $\alpha_n^4 \rightarrow 0$, $G_K \alpha_n^4 \rightarrow \tilde{G}_K$
5. 18 \rightarrow 17: $K_{\alpha_h} \rightarrow \infty$

$$6. 17 \rightarrow 16: K_{\beta_h} \rightarrow 0$$

$$7. 16 \rightarrow 15: G_{Na} \rightarrow \infty, \alpha_h \rightarrow 0, G_{Na}\alpha_h \rightarrow \tilde{G}_{Na}$$

$$8. 15 \rightarrow 14: G_L \rightarrow 0, E_L \rightarrow \infty, G_LE_L \rightarrow I_L$$

$$9. 14 \rightarrow 13: K_{\alpha_m} \rightarrow 0$$

$$10. 13 \rightarrow 12: G_{Na} \rightarrow 0, E_{Na} \rightarrow \infty, G_{Na}E_{Na} \rightarrow I_{Na}$$

$$11. 12 \rightarrow 11: V_{\alpha_m} \rightarrow -\infty, \alpha_m \rightarrow 0, \alpha_m V_{\alpha_m} \rightarrow \tilde{\alpha}_m$$

$$12. 11 \rightarrow 10: \alpha_m \rightarrow \infty, \beta_m \rightarrow \infty, m \rightarrow m_\infty, \beta_m/\alpha_m \rightarrow \tilde{\beta}_m$$

$$13. 10 \rightarrow 9: V_{\beta_h} \rightarrow -\infty$$

This limit eliminates voltage-dependence for the gating variable h , making it solely time-dependent.

$$14. 9 \rightarrow 8: G_K \rightarrow 0, E_K \rightarrow \infty, G_KE_K \rightarrow I_K$$

$$15. 8 \rightarrow 7: \beta_h \rightarrow 0, h_\infty \rightarrow 1$$

$$16. 7 \rightarrow 6: I_L \rightarrow 0$$

$$17. 6 \rightarrow 3: \text{Removing Dimension}$$

We describe briefly the process of obtaining the dimensionless reduced limit cycle model in Appendix A.6 from the reduced limit cycle model in Appendix A.5. First, we pick a convenient definition for dimensionless voltage $v = (V - V_{\beta_m})/K_{\beta_m}$. Next, we solve to find an appropriate definition for dimensionless time. Rearranging parameters in the two remaining differential equations and changing gating variables from n to w , where $w = (\beta_n/K_{\beta_m})n$, we

find a redefinition of dimensionless time $\tau = (I_K K_{\beta_m}^3 / \beta_n^4) t$. This recovers three dimensionless parameters:

$$\theta_1 = \frac{I_{Na}}{I_K} \left(\frac{\beta_n}{K_{\beta_m}} \right)^4 \quad (\text{B.11})$$

$$\theta_2 = \frac{V_{\beta_m} - V_{\alpha_n}}{K_{\beta_m}} \quad (\text{B.12})$$

$$\theta_3 = \frac{K_{\beta_m}}{I_K} \left(\frac{\beta_n}{K_{\beta_m}} \right)^4 \quad (\text{B.13})$$

Alphabetical Index

Fisher Information Matrix, 11, 20

future work, 21

geodesic, 10, 12

ideal gas, 2

Julia programming language, 11

Levenberg-Marquardt, 13

local sloppiness, 20

MBAM, 9

model

 manifold, 10

 sensitivities, 17

neuron, 3

sloppy models, 5, 10